Chapter 5

Analysis of results from thermal models: the observed albedo distribution of NEAs and the correlation of η with the phase angle

5.1 Foreword

This chapter is devoted to the analysis of results obtained from thermal model fits to the measured infrared fluxes of the NEAs observed in this study. Additional published radiometric diameters and albedos have been included to our data set. The albedo distribution of the observed NEAs is derived and correlation of albedos with taxonomic classes discussed.

Our data indicate a correlation of the NEATM best-fit parameter η with the phase angle. A linear dependence of the η-value versus the phase angle α, i.e. $\eta = (0.011\pm0.002)\alpha + (0.92\pm0.07)$ appear to describe the apparent color temperature of NEAs with common thermal properties. Some objects, however, with very low color temperature have been identified.

Furthermore, there is evidence that the slope of this linear function depends on the albedo of the objects, with the darker object of the C-complex having a steeper slope than the asteroids of the S-complex with higher albedo. This linear function can be used to estimate the default η-value in those cases where η cannot be constrained by a proper fit of the measured thermal infrared spectral energy distribution. This refinement to the default η value for the NEATM, produces infrared phase curves which are in agreement with observations of main belt asteroids and the NEA 433 Eros in the range $0°<\alpha<30°$.

Our data set allows the thermal phase function of asteroids to be studied up to 80° of phase angle for the first time.

Comparison of STM-derived radiometric diameters with diameters estimated from radar allows a possible calibration of the STM for use with NEAs. I show that the use of the refined NEATM or the radar calibrated STM is equivalent to analyze radiometric observations up to 45° - 50° of phase angle.

5.2 The observed albedo distribution of NEAs

The mean albedo of the 32 objects observed in this program is 0.27 and it does not change when the mean albedo is calculated for all (46) asteroids with reliable radiometry listed in Table 4-6. This value is much higher than the mean albedo of all main-belt asteroids listed in the Supplemental IRAS Minor Planet Survey, SIMPS, database (Tedesco et al., 2002) which is around 0.1.

Tedesco et al. (2002) noted a different albedo distribution (see plot mean albedo vs. diameter), between the newly identified IRAS asteroids of the SIMPS and the original IMPS objects. The authors claim that this marked difference is due to a discovery bias in favor of objects being brighter in a magnitude limited discovery-survey. This might be our case as well. Luu and Jewitt (1989) describe how

a bias factor in favor of the discovery of S-type NEAs is important in defining the taxonomic type distribution of this population (see section 1.3 and Fig. 1.3 of this work and Binzel et al., 2002, for further details). Given their higher albedo, in limited magnitude surveys, S-type asteroids are more likely to be discovered. Moreover, the fall off of the apparent brightness of the darker C-types as a function of the solar phase angle is stronger than for S-types.
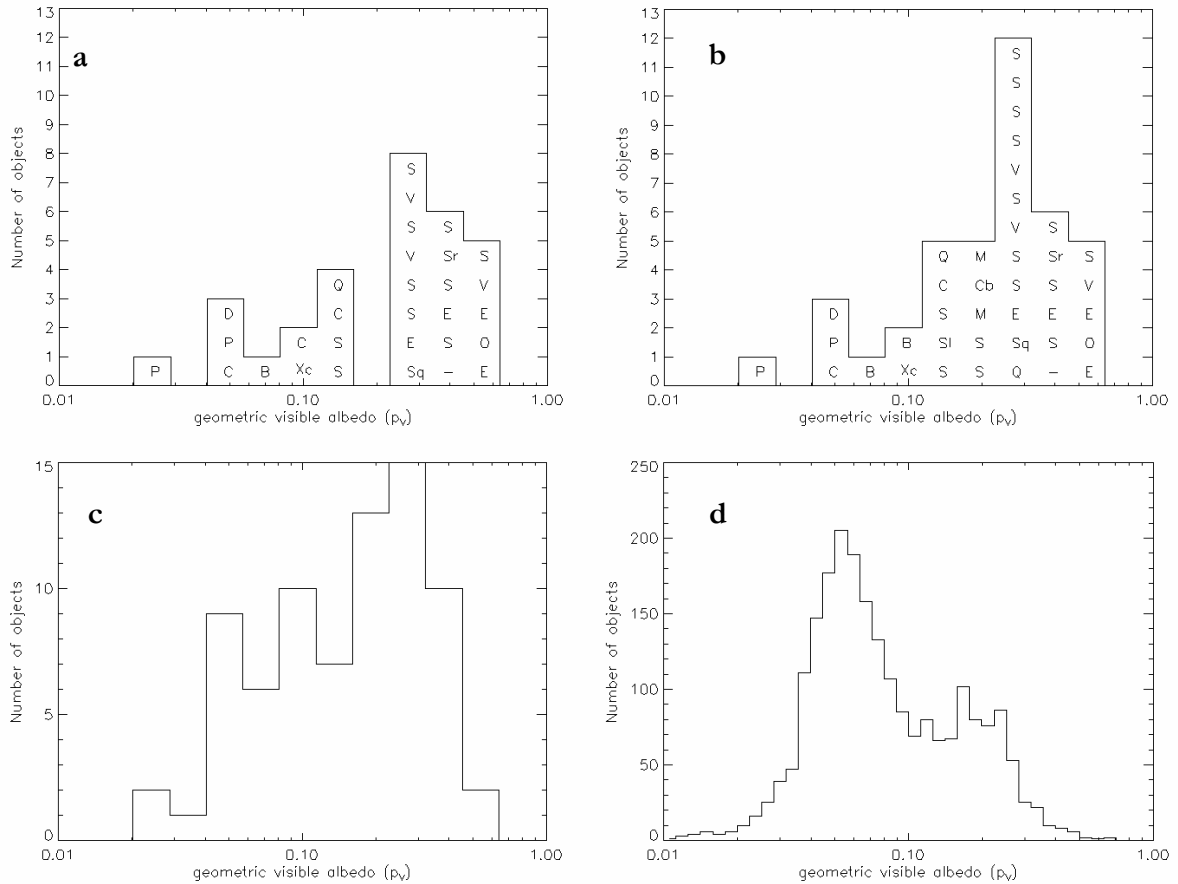

Fig. 5.1 Comparison of albedo distribution for the NEAs observed in this program (histogram **a** which contains 30 NEAs); all NEAs with radiometric reliable albedo (histogram **b** with 40 objects); SIMPS asteroids with diameter less than or equal to 10 km (**c** with 75 asteroids) and all SIMPS asteroids (**d**, with 2228 objects). In the first three histograms bins are 0.15-wide in logarithmic albedo, whereas in the last one they are 0.05-wide in logarithmic albedo. In the case of NEAs and SMASSII-asteroids the taxonomic class is displayed.

Therefore, since NEAs are often discovered at large phase angles, the coupling of the two effects might explain the lack of dark objects within the population known so far.

Fig. 5.1 shows the albedo distribution of the NEAs observed in this program (plot a) and of all NEAs for which reliable radiometric albedo is available (plot b) compared to that of all SIMPS asteroids

(plot d). We can notice in the NEA population the lack of dark asteroids with $p_V < 0.10$ which are the majority in the main belt population. 87% of the NEAs have albedo greater than or equal to 0.1. In the SIMPS database those asteroids with $p_V \geq 0.1$ are only 34%. The maximum of the NEA albedo distribution peaks in the bin roughly between p_V 0.2 and 0.3, whereas in the case of main belt asteroids the maximum lies at about $p_V = 0.06$. Moreover, the distribution of the albedos for only the S-type asteroids is different in the NEA population than in the main belt: MBAs are on average darker.

However, by comparing the SIMPS database with results obtained in this work, we are looking at asteroids which are on average dramatically different in size. Constraining the analysis to SIMPS asteroids with diameter smaller than or equal to 10 km (Fig. 5.1, plot e), about 70% of the objects are found to have p_V larger than 0.1 and the apparent albedo distribution plot is more similar to that derived for the NEA population (the maximum of the these two distributions, for example, falls in the same albedo-bin).
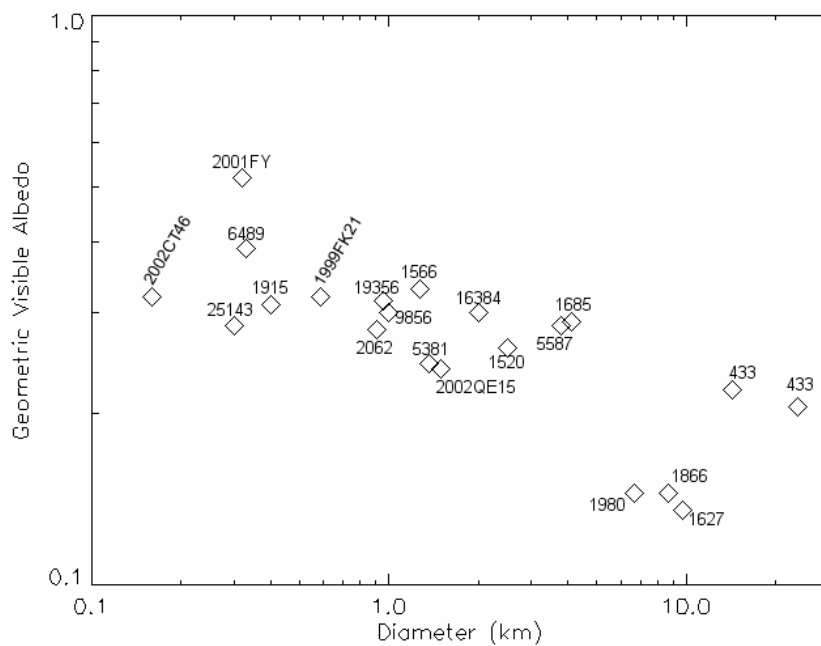

Fig. 5.2 Plot of the geometric visible albedo versus diameter derived by NEATM for S-type NEAs. Taxonomic classes included are 'S', "Sq', 'Sr' and 'Sl'. The plot suggests a significant trend of increasing albedo with decreasing size. The trend may be due to a bias in favor of the discovery and characterization of high albedo objects. In the case of 433 Eros results are shown at lightcurve maximum and minimum.

The apparent size dependence of the albedo in the IRAS data has been discussed by a number of workers and attributed to the lack of dusty regolith on small asteroids (see Tedesco, 1993). A rocky

surface should have a larger thermal inertia than that of a surface with a dusty regolith, thus causing the STM with its fixed value of 0.756 for the model parameter η to give erroneously high albedos.

We are aware that STM (with the fixed η-value of 0.756) produces radiometric albedos higher than the true value, if thermal inertia and rotation rate plays an important role in modifying the surface temperature distribution of small asteroids. Clearly, this effect is particularly important for NEAs which are observed at high phase angle (see Chapter 6). By using the NEATM, which adjust the η-value, we take into better account the modification to the surface temperature caused by the thermal inertia and rotation rate of NEAs. As we demonstrate in Chapter 6, NEATM albedos and diameters are more reliable than the ones derived by the STM. Nevertheless, objects with high albedo are the majority in our data base.

Moreover, albedos of the observed NEAs are not only on "average" higher than that of MBAs, but correlation of the albedo with size exists within the NEA population itself.

In Fig. 5.2 the albedos of 21 S-type NEAs are plotted against effective diameters. Our data suggest a trend of increasing albedo with decreasing size in agreement with Delbò et al. (2003) results. If this trend is real, it may be indicative of lack of space weathering on the recently exposed, relatively young surfaces of small objects.

However, a selection effect in favor of the discovery of brighter NEAs in a magnitude limited survey may explain such trend. A simulation of the NEA discovery process and the possible selection effect involved in the choice of the objects to be observed in the thermal infrared is an important future work that can clarify this issue.

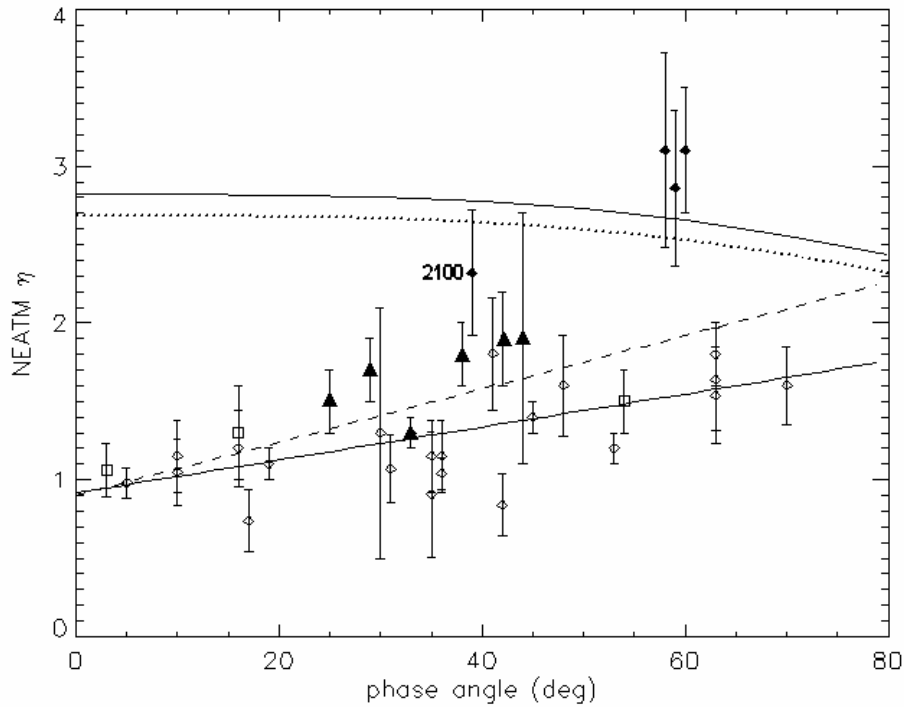## 5.3   Phase angle dependence of the observed color temperature

Fig. 5.3 Best-fit beaming parameter, η, from the NEATM fits plotted against solar phase angle, α. The continuous line represents a linear fit, $\eta = (0.011\pm0.002)\alpha + (0.92\pm0.07)$ to all values of η. Filled diamonds with error-bars at $\eta>2$ are those data points considered anomalous by Delbò et al. (2003). Filled triangles are the η-values for 5381 Sekmeth and the dashed line represent their linear fit: $\eta = (0.017\pm0.013)\alpha + (0.9\pm0.03)$. Open squares represent the η-values for 25330 (1999 KV$_4$). Significant deviations of η from the linear fit may be due to the effects of unusually high or low thermal inertia and/or surface roughness, and/or an irregular shape, influencing the surface temperature distribution presented to the observer. The "evening/morning" effect probably contributes to the scatter of the points (see text). The dotted curve represents the expected η values for an FRM-like asteroid, whereas the continuous one corresponds to the η-values derived by fitting NEATM to the infrared continuum of a perfectly conducting smooth sphere in thermal equilibrium with the solar radiation.

Fig. 5.3 shows a plot of the η-value derived by the NEATM versus phase angle based on the results of this study and previously published results given in Table 4-6. The η-value represents the fourth power of the ratio between (1) the color temperature that an observer would derive for a smooth non-rotating sphere with each point of its surface in equilibrium with insolation and thermal emission, and (2) the actual color temperature derived from observations with both objects observed at the same phase angle: i.e.:

$$\eta = \left(\frac{T_{EQ}}{T_C}\right)^4 \tag{5-1}$$

It is clear that in the case of the observed NEAs the derived η is usually significantly larger than the value $\eta=0.756$ used in the STM of Lebofsky et al. (1989) and derived on the basis of observations of 1 Ceres and 2 Pallas. The larger η-values, compared with the value of 0.756 used in the IRAS STM for main-belt asteroids, are consistent with the results of previous authors suggesting that NEAs have larger surface thermal inertias in general than main-belt asteroids.

Moreover, the plot suggests a significant trend of increasing η-value with increasing solar phase angle and a bimodal η distribution at phase angles larger than $\sim30°$. While the majority of objects display relatively high color temperatures (low η) even at solar phase angles as large as 60-70°, a number of cases with η-values significantly larger have been found, indicating unusually low color temperatures for their surfaces.

5.3.1 NEAs with anomalous thermal properties ($\eta>2$)

In those cases with $\eta>2$ (shown in Fig. 5.3 with filled black diamonds and already identified by Delbò et al, 2003 as "anomalous"), the FRM best fits to the observed thermal continua are reasonably good, suggesting that the temperature distributions around the surfaces of these objects may be relatively smooth, with significant emission arising on the night side, due to high thermal inertia and/or high rotation rates. However, it is remarkable to note that two of the three objects with the highest η-values, namely 3671 Dionysus[19] and 2002 BM_{26}, are fast rotators with periods around 2.7 hours. On the other hand, the other two high-η objects, namely 2100 Ra-Shalom and 1999 NC_{43}, are slow rotators (with periods of 19.8 h and at least 34 h, respectively). If their temperature distributions are well described by the FRM, Ra-Shalom and 1999 NC_{43} must have exceptionally high surface thermal inertias comparable to, or exceeding, that of solid rock (2500 J/m^2 s/$^{0.5}$ /K^1, Jakosky, 1986).

The presence of objects with η larger than 2, with very different rotational period and the evidence for a bimodal distribution of η-values at moderate and large phase angles, suggest that the interpretation of the large η-values in terms of rotation rate and thermal inertia is an oversimplification.

Moreover, Fig. 5.3 suggests that in general the FRM does not describe properly the thermal characteristics of the asteroids in our database. The dotted line intersecting the η-axis at the value of 2.6

---

[19] The FRM solution for 3671 from Harris and Davies (1999) requires $p_V > 0.3$, which is inconsistent with the taxonomic class Cb from Bus and Binzel (2002).

and decreasing towards larger phase angles represents the η-value expected for an FRM-like asteroid. The fact that the η-values derived from our observations are in the majority significantly below the dotted line is and indication that the FRM implies a color temperature which is too low with respect to that derived for the asteroids in our database. On the other hand, it is remarkable that the color temperature derived for 3671 Dionysus, 2002 BM_{26} and 1999 NC_{43} are significantly lower that the one implied by the FRM. In the case of 1999 NC_{43}, which has a high amplitude lightcurve indicative of a very irregular shape, the explanation for the high η-value may lie in shape or shadowing effects that lead to less thermal emission being received from the observed parts of the surface than predicted by the spherical geometry on which the simple thermal models are based (see Delbó and Harris, 2002). The importance of such effects increases with phase angle.

It is remarkable that even a perfectly conducting smooth sphere (PCSS), in thermal equilibrium with the solar radiation, would display a color temperature warmer (lower η-value) than the ones derived for 3671 Dionysus, 2002 BM_{26} and 1999 NC_{43}. In fact the η-value that the NEATM would derive by fitting the thermal infrared continuum of a PCSS follows the continuous line drawn in Fig. 5.3 intersecting the η axis at the value of 2.82.

5.3.2 NEAs with "common" thermal properties

It is clear that the majority of objects display relatively high color temperatures (low η) even at solar phase angles as large as 60-70°. Delbò et al. (2003) noted that a linear function can describe the dependence of the η-values with phase angle for NEAs with "common" thermal properties. They have fitted a straight line to the points with η<2 separating out the four points with η>2 and derived a dependence of the η-value as a function of the phase angle α such that η=0.01α+0.81. Here, I have included in the analysis new results from the ESO and the NASA-IRTF observation campaigns. Excluding objects with "anomalous" color temperature (η>2) I have obtained the best linear fit of η= (0.009±0.002)α+(0.89±0.07). Given the uncertainties, the fit is in good agreement with the one by Delbò et al. and the η-value at zero degree of phase angle is slightly larger than the one obtained by Delbò et al. and significantly higher than that adopted by Lebofsky et al (1986) for use in the STM. Including also those points with η>2 the slope of the linear fit and its value at α=0° become slightly larger: i.e. η=(0.011±0.002)α+(0.92±0.07), though, given the error bars of the data points, both results are still in good agreement.

If we express the phase angle dependency of the η-value with the linear relation $η = β_η α + η_0$, our data-set suggests the evidence for the $β_η$ and the $η_0$ parameters to be a function of the object albedo. For

the brightest objects i.e. those with $p_V>0.25$ the best linear fit is obtained with $\beta_\eta=0.006\pm0.002$ and $\eta_0=1.0\pm0.1$. A significant different value for the β_η parameter i.e. $\beta_\eta=0.016\pm0.003$, but with η_0 only slightly smaller ($\eta_0=0.8\pm0.1$) can be derived for those objects with $p_V<0.25$. If we consider only dark objects ($p_V\leq0.1$) the slope of the linear fit keeps at the constant value $\beta_\eta=0.016\pm0.006$, while the value of η_0 decrease to 0.6 ± 0.2. This latter result might be somewhat questionable given the low number of data points (four) included in the linear fit.

The above results indicate that the linear relation $\eta=(0.011\pm0.002)\alpha+(0.92\pm0.07)$, can give the best default value for η as a function of the phase angle to use with NEATM when data at only one or two thermal wavelengths are available and spectral fitting is not possible. Clearly such a relation allows the NEATM to be used to make more accurate prediction of the expected infrared flux from an asteroid, provided it has "common" thermal properties.

5.4 The infrared phase curve of NEAs with "common" thermal properties

It is known from observations that asteroids show infrared phase curves which are approximately linear in the range 0-30° with slopes of about 0.01 mag/degree Morrison, 1976; Matson, 1971; Lebofsky and Spencer, 1989). Moreover, Murdock, 1974 noted that in the case of Mercury, the curves of measured effective brightness temperature as a function of phase angle are steeper than those of a smooth sphere.

In this section it is shown that the infrared phase curves of NEAs with "common" thermal properties – i.e. those with an η-value following the linear function derived in the section 5.3.2 – are steeper, than those of a Lambertian emission model and in better agreement with observations. Fig. 5.4 shows infrared phase curves (the magnitude scale is set equal to zero at $\alpha=0^\circ$) calculated at $\lambda=11.7\mu m$ for a spherical asteroid at the heliocentric distance of 1AU. The temperature distribution on the surface of the object is described by the formula of thermal equilibrium with solar radiation at each point: i.e.

$$T_{SS}=\left(\frac{1}{r^2}\frac{S_\oplus(1-A)}{\sigma\varepsilon\eta}\right)^{1/4}$$

$$\begin{cases}T(\theta)=T_{SS}[\cos(\theta)]^{1/4} & \text{for } \theta<\pi/2 \\ T(\theta)=0 & \text{for } \theta\geq\pi/2\end{cases}$$

(5-2)

where θ is the sub-solar colatitude. The total radiated flux $F(\lambda)$ is obtained, as usual, by integrating numerically the actual thermal flux an observer would detect from the illuminated portion of the sphere

visible to him at the given solar phase angle (for further details see Delbo & Harris, 2002 Eqs. 19-21). However, the η-value is assumed here to be a linear function of the solar phase angle α with the law

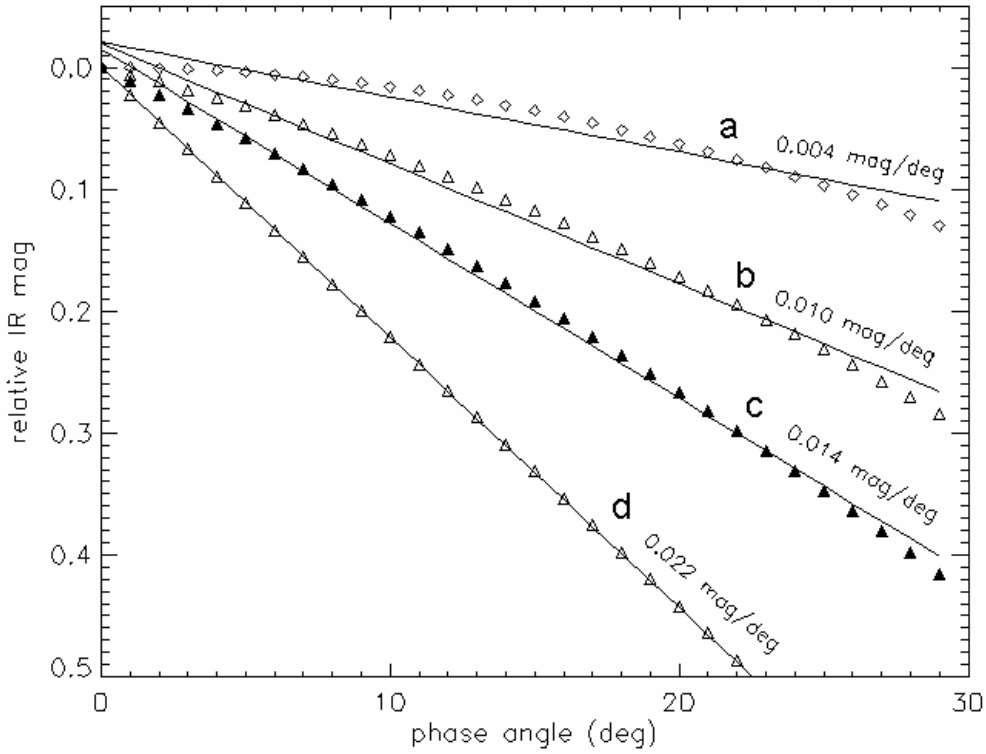$$\eta = \beta_\eta \times \alpha + \eta_0 \qquad\qquad\qquad (5\text{-}3)$$

Fig. 5.4 Infrared phase curves for a spherical asteroid at the heliocentric distance of 1AU with a STM-like temperature distribution. However, the η-value is varied as a linear function of the phase angle α: $\eta = \beta_\eta \alpha + \eta_0$. See the text for further details.

The topmost curve, the one labeled with "**a**", in Fig. 5.4 was calculated for $\beta_\eta = 0$ and $\eta_0 = 1$ (i.e. $\eta = 1$ and constant for every α). This curve is not sensitive to changes of η_0. Objects at different heliocentric distance would thus display the same phase curve. Curve "**b**" was calculated for $\beta_\eta = 0.006$ and $\eta_0 = 1.0$, curve "**c**" for $\beta_\eta = 0.011$ and $\eta_0 = 0.92$, curve "**d**" for $\beta_\eta = 0.016$ and $\eta_0 = 0.6$. The straight line passing through the points is the best linear fit in the range $\alpha = 0°\text{-}30°$ to the model curves. The slope of this linear fit is the equivalent of the thermal phase coefficient, β_E, that Lebofsky and Spencer (1989) and Matson (1971) have derived for main-belt asteroids. A phase angle dependence of the η-value, as the one obtained in this work, yields a steeper phase function than the one obtained by assuming Lambertian emission at the surface of the asteroid. Table 5-1 shows the value of β_E at 11.7 μm for different values of β_η and η_0 for an asteroid at 1 AU from the Sun.

β_η	η_0	β_E (mag/deg)	*Note*
0	1.0	0.004	Lambert
0.006	1.0	0.010	$p_V > 0.25$
0.011	0.92	0.014	mean value
0.016	0.60	0.022	$p_V < 0.1$

Table 5-1 The infrared phase coefficient, β_E, obtained as a linear fit to the phase curves produced by using the NEATM

Matson (1971) observed that main-belt asteroids had solar phase coefficient β_E in the thermal infrared that ranged from about 0.005 to 0.017 mag/deg. A mean value of 0.01 mag/deg has been used in the STM to correct measured thermal fluxes to the zero phase assumed by this model (Lebofsky and Spencer, 1989). Morrison (1976) analyzed infrared observations of 433 Eros obtained at $\alpha < 40^\circ$ before and after opposition and obtained an infrared phase slope of about 0.008 mag/deg. This value is in good agreement with the lunar-type model for 4 Vesta computed by Matson (1972).

The linear relation of the η-value may be used as the default value for η when it is not possible to derive it via a fit of the thermal infrared continuum. Such relation determines a dependence of the infrared flux with phase angle which mimics, in the range $0° < \alpha < 30°$ the measured phase curves of main belt asteroids and of 433 Eros. The mean value for slope of the infrared phase curve is 0.011 mag/deg in the case of those NEAs analyzed in this work.

5.5   Comparison of radiometric diameters with radar

Uncertainties in thermal modeling usually exceed the formal errors resulting form the scatter of the flux measurements. Comparison of diameters derived by means of other techniques such as radar offers the opportunity to test the thermal models we have adopted and estimate the overall errors involved in their use. In this section the relative error between radiometric diameters ($D_{radiometry}$) and radar diameters (D_{radar})- i.e. ($D_{radiometry}$-D_{radar})/D_{radar}, has been calculated for those asteroid for which size estimates are available from radar observations. Original source for each radar diameter is given in Table 4-6. The error bars of Fig. 5.5, Fig. 5.6 and Fig. 5.7 were calculated assuming a 15% uncertainty on radiometric diameters and the formal error of radar sizes, σ_{Dradar}. A 15% uncertainty on radar diameters was also assumed in those cases where the diameter error is not available from the original source. The formal error of the quantity "relative diameter error" is given by Eq. 5-4.

$$\sigma_{relative\_diameter\_error} = \sqrt{\left(\frac{0.15 * D_{radiometry}}{D_{radar}}\right)^2 + \left(\frac{\sigma_{D_{radar}} D_{radiometry}}{D_{radar}^2}\right)^2} \ , \tag{5-4}$$

For those asteroids with radiometric observations available at different geometries, the relative diameter error was calculated for each observation. For example, three data points are drawn for the asteroid 433 Eros. In that case radiometric measurements were obtained at lightcurve maximum and at lightcurve minimum and at two different phase angles, namely 10° and 31°.

Fig. 5.5: Comparison of STM diameters with radar ones as a function of the solar phase angle (a) and diameter (b) for those asteroids observed at phase angles less than or equal to 80°. For 433 Eros results are given at lightcurve maximum and at lightcurve minimum. A systematic error of -16% is evident between the two sets of data. The RMS fractional difference between the STM diameters and diameters derived from radar measurements is of 16%. No clear trend of the relative error with phase angle is evident. Error bars were calculated assuming a 15% uncertainty on STM radiometric diameters and 10% uncertainty on the radar one if such information was not available from the original source in the literature. The thick continuous line on plot (a) and (b) was obtained with a 6-elements central running box average. Plot (c) shows the histogram of the relative error distribution with superimposed the mean and the median values. Plot (d) shows how STM diameters are in good agreement with radar ones if asteroids 2100, 1580, 6489 and 33342 are removed from the sample.

The radiometric diameter of 6489 Golevka is a new value derived by applying the thermal models to infrared observations obtained at the NASA-IRTF during the June 2003 apparition. Although the new observations have been obtained at a phase angle of 43°, a value much smaller the extreme case of 90° at the time of Mottola et al. (1997) UKIRT observation, the radiometric diameter is still almost 40% smaller (in the case of the NEATM and the STM) than the value derived by the radar.

In Fig. 5.5 the relative diameter errors of the STM are plotted against phase angle and size. STM-derived diameters are on average significantly smaller than radar diameters: a systematic error with a mean difference of about 16% and an RMS fractional difference of 16% is evident between the two sets of data. This latter value is in good agreement with the typical STM diameter uncertainty of 15% that we have assumed as the result of thermal modeling. No clear trend of the error with the phase angle is visible, although from the plot (b) of Fig. 5.5, it looks like that the STM gives more accurate diameters in the case of large NEAs. It is worth to point out that the NEAs 2100 Ra-Shalom, 1580 Betulia, 6489 Golevka and 33342 (1998 WT$_{24}$) carry the largest contribution to the deviation from the mean and the median value of the distribution from zero and appear to have STM radiometric diameter significantly smaller than the radar ones. In fact, the mean difference between STM derived diameters and radar one reduces to -5% with RMS equal to 6% if those asteroids are excluded. This might be an indication that the STM fails to reproduce the thermal properties of those asteroids. In fact, large η-values have been derived in those cases, which is an indication of low color temperature. The STM fits to the thermal continua measured for those asteroids is poor. It is possible that shadowing or shape effects may invalidate the application of simple thermal models in such cases (see Delbó and Harris, 2002), and it is clear that an alternative explanation to that of having large thermal inertia has to been considered for those objects (see section 5.3.1).
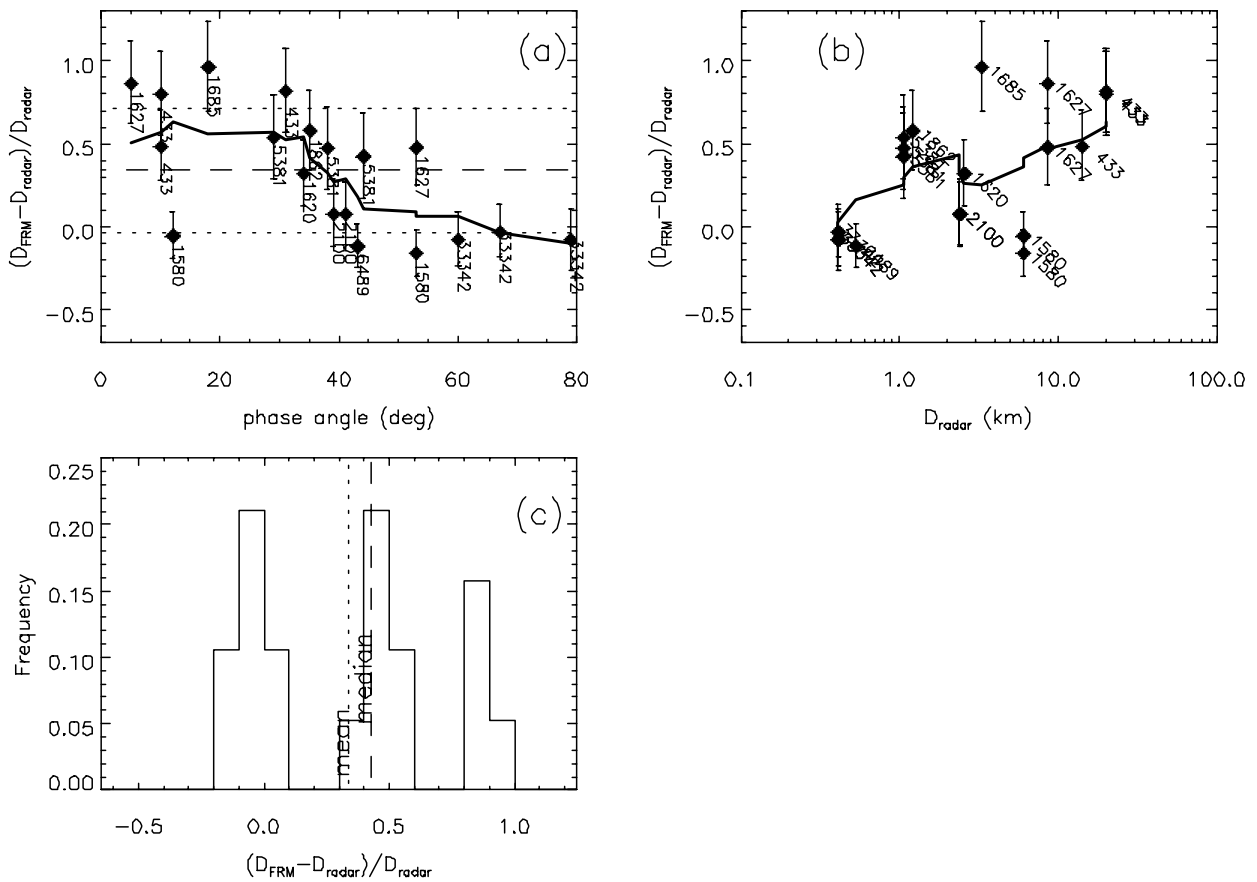
Fig. 5.6 Comparison of FRM diameters with radar ones as a function of the solar phase angle (a) and diameter (b) for those asteroids observed at phase angles less than or equal to 80°. For 433 Eros results are given at lightcurve maximum and at lightcurve minimum. A systematic error of +35% is evident between the two sets of data. The RMS fractional difference between the FRM diameters and diameters derived from radar measurements is of about 40%. There is a clear trend of the relative diameter error with the phase angle and with the diameter. Error bars were calculated assuming a 15% uncertainty on FRM radiometric diameters and 10% uncertainty on the radar one if such information was not available from the original source in the literature. The thick continuous line on plot (a) and (b) was obtained with a 6-elements central running box average. Plot (c) shows the histogram of the relative error distribution with superimposed the mean and the median values.

A large discrepancy between radar and FRM-derived diameters is clearly visible in Fig. 5.6. A correlation of the diameter errors with the phase angle is evident even excluding asteroids 2100, 1580, 6489 and 33342 for which the FRM produces results consistent with radar ones. It is remarkable that the FRM fails to reproduce radar diameter for those asteroids which were observed at low or moderate phase angle.
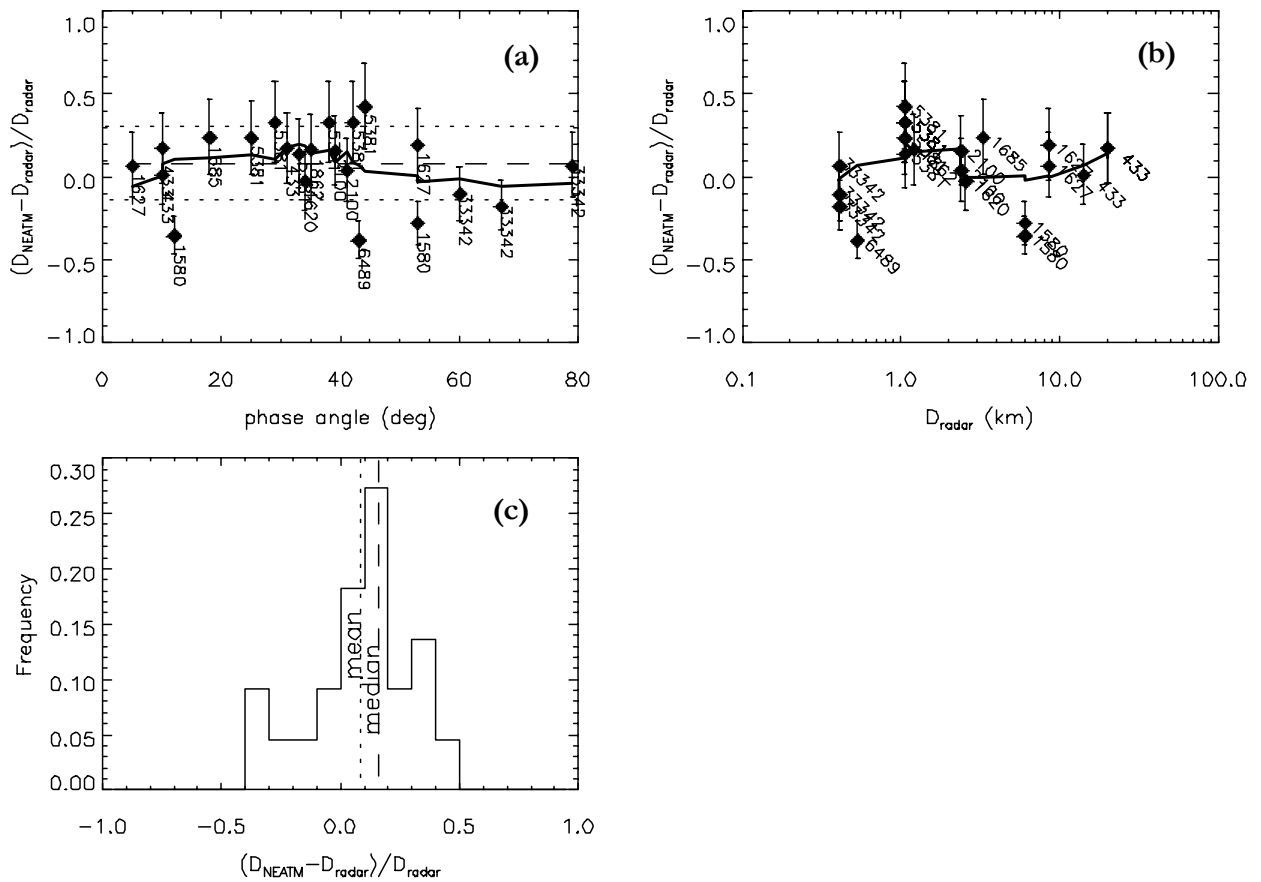
Fig. 5.7 Comparison of NEATM diameters with radar results as a function of the solar phase angle (a) and diameter (b) for those asteroids observed at phase angles less than or equal to 80°. For 433 Eros results are given at lightcurve maximum and at lightcurve minimum. A systematic error of +8% is evident between the two sets of data. The RMS fractional difference between the STM diameters and diameters derived from radar measurements is of about 20%. No clear trend of the relative error with phase angle and size is evident. Error bars were calculated assuming a 15% uncertainty on STM radiometric diameters and 10% uncertainty on the radar one if such information was not available from the original source in the literature. The thick continuous line on plot (a) and (b) was obtained with a 6-elements central running box average. Plot (c) shows the histogram of the relative error distribution with superimposed the mean and the median values.

In Fig. 5.7 NEATM relative errors with respect to radar diameters are plotted as a function of the phase angle and the diameter. The mean relative error is of +8% between the two sets of data. The RMS fractional difference between the NEATM diameters and diameters derived from radar measurements is of 20%. A gaussian function of the form $A \times \exp(-(x-x_0)^2/(2\sigma)^2)$ best fits to the relative error distribution with a σ parameter equal to 0.17 and a mean value $x_0 = 0.08$. The NEATM mean relative error of 0.08 ± 0.04 (the error of the mean is $\sigma/\sqrt{N}$) is therefore significant and indicates a systematic error between radar and NEATM diameters.

104

5.6   On the recalibration of the STM for NEAs

Comparison of STM-derived radiometric diameters with diameters estimated from radar observations offers the opportunity to calibrate the STM for use with NEAs. Despite its simplicity STM has proved to produce diameters in good agreement with those derived from occultation measurements in the case of large main-belt asteroids (see Harris and Lagerros, 2002). However, STM results depend on the assumed η-value. In the STM of Lebofsky et al (1986) η is set equal to 0.756. This value was derived by constraining the thermal model to match the occultation diameters of 1 Ceres and 2 Pallas and their thermal infrared fluxes measured at 10 μm. η takes account of effects that alter the apparent day side temperature distribution compared to that of a perfectly smooth, non-rotating sphere, such as the enhanced sunward thermal emission due to surface roughness and the fact that in reality all asteroids rotate and thus radiate some of their thermal emission on the night side. In practice η can be considered as a normalization or calibration factor. However, there is no reason to assume that an η-value of 0.756 makes the STM to produce reliable results for all small bodies in our solar system. For example, Morrison (1973) and Morrison and Chapman (1976) determined a beaming factor of about 0.86 from stellar and lunar occultation of the Jovian satellites and of Iapetus. Spencer et al (1989) determined a disk integrated η-value of 0.72 for the Moon.
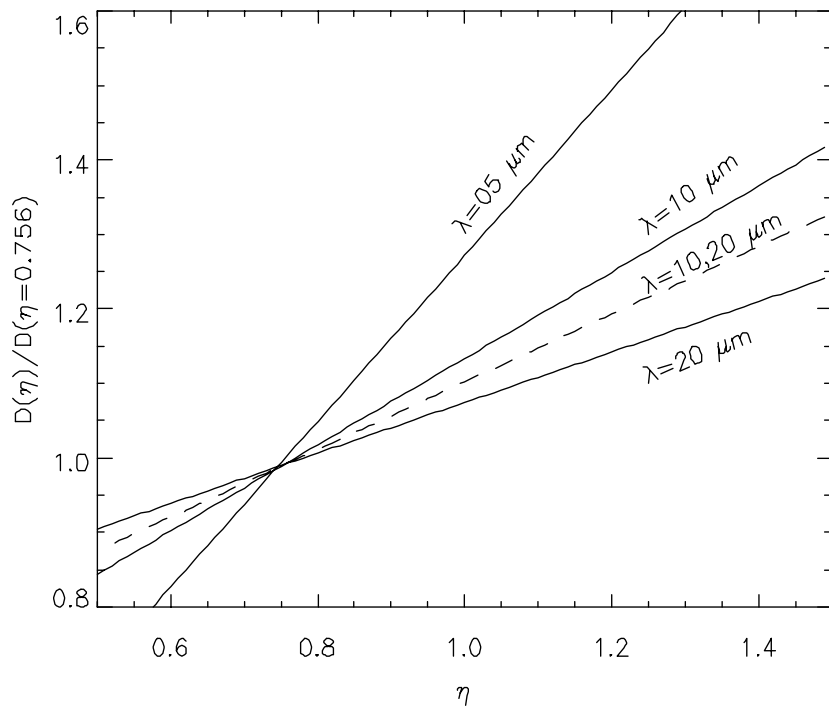

Fig. 5.8 Dependence of the STM-derived radiometric diameter at wavelengths of 5, 10 and 20 μm as a function of the beaming parameter η. Dashed line was obtained by fitting the STM simultaneously to 10 and 20 μm fluxes.

To produce the results of Fig. 5.5 the standard η-value of 0.756 was adopted. However, doing so the STM underestimates radar diameters by a factor between 5 and 15% depending on whether the asteroids 2100 Ra-Shalom, 1580 Betulia, 6489 Golevka and 33342 (1998 WT$_{24}$) are excluded.

By assuming a larger η-value STM-derived diameters become larger (and geometric albedo consequently smaller). I have studied the dependence of the radiometric diameter as a function of the model input parameter η when the STM is used to fit thermal infrared fluxes obtained at one wavelength. Fig. 5.8 shows this functional dependence: the STM-derived diameter divided by the diameter obtained by setting η equal to 0.756 is plotted against the input η value. This calculation was carried out at the wavelengths of 5, 10 and 20 µm. These results are shown with continuous lines. Dashed line was obtained by fitting the STM simultaneously to multi-wavelength fluxes obtained at 10 and 20 µm.
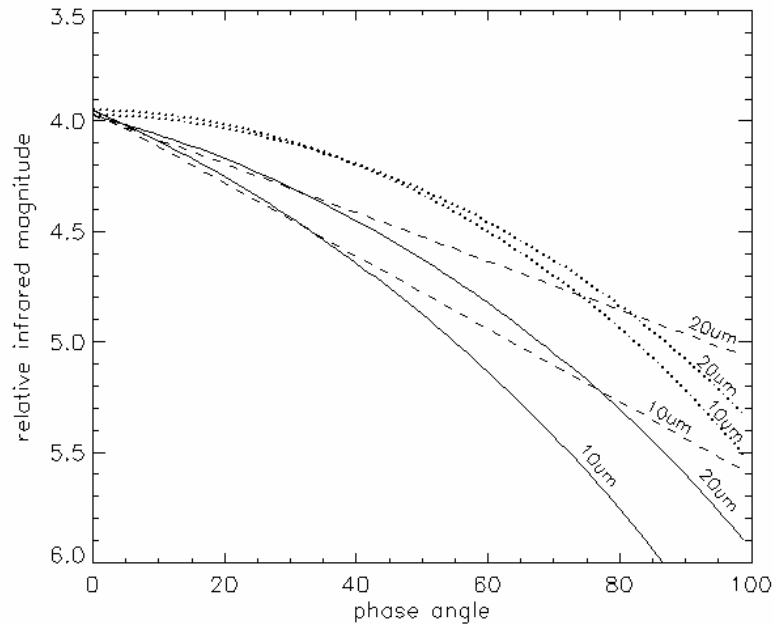

Fig. 5.9 Infrared phase curves in terms of relative infrared magnitudes for a spherical asteroid calculated at 10 and 20 µm. Continuous line: NEATM with $\eta=0.011\alpha+0.9$ where α is the phase angle and η the beaming parameter (see text). Dashed line: STM for which $\eta=0.9$ was assumed. The 10µm phase curve was obtained with a β_E-value of 0.015 mag/degree, whereas for the 20µm curve β_E was set equal to 0.011 mag/degree. Those value were chosen to fit the NEATM phase curve in the range $0°<\alpha<30°$. Dotted lines represent the phase curve of a NEATM-like asteroid with a fixed η-value of 0.9.

From Fig. 5.8 it is evident that setting η to a value between 0.85 and 0.95 yields a resulting diameter between 5 and 15% larger on average than the value the STM derives with $\eta=0.756$.

Furthermore, Fig. 5.8 shows how this calibration is a function of the wavelength at which the thermal model is used. Radiometric diameters obtained at 20μm are less sensitive to change in the η parameter (the slope of the diameter variation with η being shallower than the slope at 10μm). It is worth to remark here that an η value between 0.85 and 0.95 is close to the η_0 parameter derived in section 5.1 where the phase function of the NEATM has been studied at a wavelength of 11.7 μm. Since both the STM and the NEATM assume the same temperature distribution on the spherical asteroid, it is clear that η_0 represent the STM η value. They should have therefore the same numerical value.In Fig. 5.9 infrared phase curves were calculated at 10 and 20 μm using NEATM but forcing the η-value to change with the phase angle α according to the relation $\eta=0.011\times\alpha+0.9$ As discussed in section 5.4 those phase curves can be very well approximated in the range $0<\alpha<30$ degrees by a linear relation the slope of which is the β_E parameter. The best fit value for β_E in the range $0<\alpha<30$ degrees was found to be 0.015 mag/deg at 10 μm and of 0.011 mag/deg at 20 μm. Instead of using the standard infrared phase coefficient of 0.01 mag/deg of the STM, I have adopted the previously determined values to calculate the 10 and 20 μm infrared magnitude which have been plotted in Fig. 5.9 with dashed lines. The STM η was set to 0.9 for this calculation.

The resulting NEATM and STM phase curves are in very good agreement up to a phase angle of about 50 degrees where the error is within 0.1 magnitudes (i.e. ~10% in term of flux). At ~70° the difference between NEATM and STM phase curves approach 0.25 mag (~25% in flux) at 10 μm and about the same value at 20 μm. If thermal infrared data do not the η-value to be properly fit, in section 5.2 a default relation $\eta=0.011\times\alpha+0.9$ has been proposed. However, the use of the STM with η=0.9 and β_E=0.013 mag/deg gives results within measurement errors.

5.7   Correlation of radiometric albedos with solar phase angle

Harris (1998) showed that, in the majority of cases, neither the STM nor the FRM provide a good fit to the observed thermal infrared continuum of NEAs. In those cases, he demonstrated that a better fit to the observed spectral distribution of the energy could be achieved by using the NEATM.
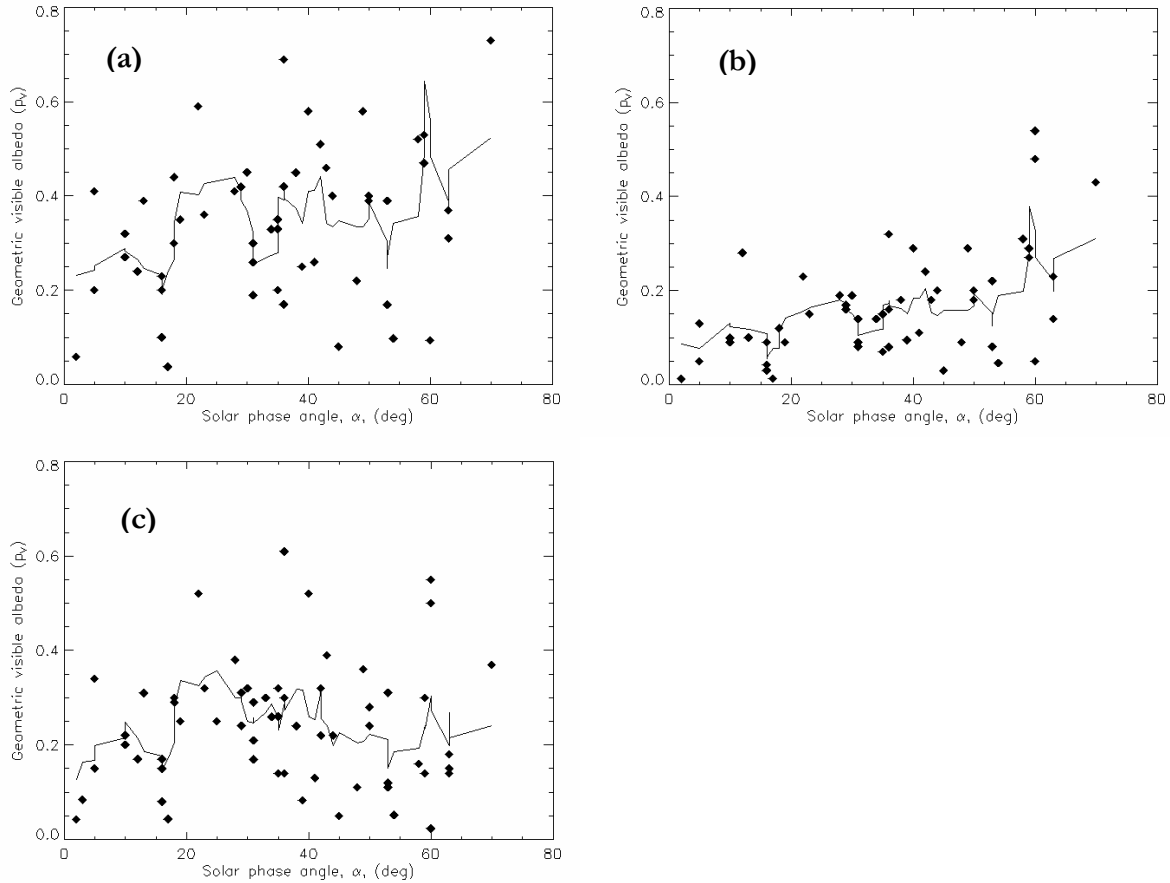

Fig. 5.10 Plot of the geometric visible albedos versus solar phase angle for each radiometric observation. a) STM; b) FRM; c) NEATM. Continuous lines were calculated by taking the 5-elements-wide central moving average of the data points in each plot.

In Fig. 5.10 plots a) and b) clearly show a second problem that affects the application of both the STM and the FRM to the study of NEAs. In that figure I have plotted the thermal model-derived albedo as a function of the solar phase angle at which each observation has been obtained. In both cases a trend of increasing albedo with increasing phase angle is visible. If the thermal model phase function does not properly account for the actual variation of the infrared flux with the phase angle, resulting diameters and albedos are correlated with this angle. Higher albedos derived at higher phase angle result from an underestimation of the infrared phase curve. It is clear that is the case of the FRM, for which no flux correction for the phase angle applies (flat model phase curve). In the case of the STM, it

108

appears the 0.01 mag/deg correction to be not large enough to account for the actual drop of infrared flux that NEAs display. Roughly speaking, plot a) of Fig. 5.10 shows that there is almost a factor of 2 increment in the average albedo in about 70° of phase angle. Since within the thermal model, diameter and albedo are constrained by the H value, the variation of the infrared flux is almost inverse proportional to variation of the albedo. A factor of 2 in terms of flux corresponds to 0.75 magnitudes, and in the hypothesis that the observed trend of Fig. 5.10 is linear, an extra term of ~0.01 mag/deg should be added to the standard β_E-value to make the STM able to account for the actual infrared phase function of NEAs.

The distribution of albedos derived by means of the NEATM appears to have no correlation with the phase angle, indicating that the procedure used to model observations at non-zero phase angle does not introduce systematic errors in the final results. I remind here what that procedure is about: In the NEATM the solar phase angle is taken account of by calculating numerically the actual thermal flux an observer would detect from the illuminated portion of a smooth sphere visible to him at a given solar phase angle, assuming that the night side does not irradiate. Further, the model temperature is modified, by changing η, to force consistency with the observed apparent color temperature of the asteroid. In those cases where the infrared data are not good enough for η to be constrained properly, η is assumed to be equal to 1 for phase angles less than 45° and equal to 1.5 beyond that value. However, one of the crucial issues concerning the reliability of the NEATM is to assess the error incurred by ignoring thermal emission from the night side. Ignoring the night side flux causes the resulting diameter to be overestimated and the albedo consequently underestimated. If such en error had played a major role, one would expect to see a trend of decreasing albedos with increasing phase angle. Results of this work indicate that this is not the case up to $\alpha \sim 60°$.

5.8 Conclusions

The beaming parameter, η, is phase-angle dependent and, on average, significantly higher than the value 0.756 adopted by Lebofsky et al. (1986) in their version of the STM. The best linear fit to the derived η values is:

$$\eta = (0.011 \pm 0.002)\alpha + (0.9 \pm 0.07) \tag{5-5}$$

where α is the phase angle. A refinement of the NEATM is proposed by using the linear relation (5-2) when it is not possible to derive η via a fit of the thermal infrared continuum. However, $\eta \sim 0.9$ appears to be valid at phase angles approaching zero, where the uncertainties associated with use of the STM are

at a minimum. This suggests that the assumption of the STM of low thermal inertia may be valid in most cases.

The phase angle function of the η value appears to be dependent on the asteroid albedo. Darker objects have steeper β_η slopes and lower η_0 values. So, high albedo objects have a less-pronounced beaming effect i.e. η_0 values closer to unity and less dependence of η on phase angle. We argue that the less-pronounced beaming effect might be due to their relatively lower equilibrium temperatures. This fact explains why, even at high phase angles, η could remain low (e.g. the case of the NEA 5587). An alternative explanation is that darker objects have more pristine and rougher surfaces leading to a stronger beaming effect than objects with higher albedos.

The fact that our sample contains no object observed at a low phase angle for which η is large (> 1.2) suggests that NEAs with high thermal inertia (i.e. regolith-free surfaces) are uncommon. One of the objects among the NEAs observed to date that may have a high thermal inertia is 2100 Ra-Shalom (η = 2.3, α = 39°). On the other hand, the very large values of η obtained for three objects observed at high phase angles (~ 60°) may be due to unusual surface structure giving rise to a strong sunward beaming effect and/or shape effects causing shadowing, rather than high thermal inertia.

In section 5.4 the thermal infrared phase curve of a refined-NEATM-like asteroid is calculated. It is worth that this infrared phase curve is linear in the range 0°-30° with a slope ~0.015 mag/deg as supported by observations of main belt asteroids.

Radiometric diameters have been compared with those obtained from radar observations. On average NEATM appears to overestimate diameters of about 10% with a RMS fractional difference of 20% from radar derived NEA sizes. A large discrepancy of FRM-derived diameters with radar ones have been shown. A strong correlation of the diameter error with phase angle, α, is evident with this error being larger for α approaching zero. The fact that the FRM fails at low phase angles supports the conclusion that high-thermal inertia surfaces are uncommon amongst NEAs.

Comparison of STM-derived diameters with diameters estimated from radar measurements allows the STM to be calibrated for use with NEAs. The STM with the standard η-value equal to 0.756 of Lebofsky et al (1986) underestimate radar diameters by about 10%. I have shown how a larger η value of ~ 0.9 allows the STM to derive asteroid diameters in better agreement with radar results. It is worth pointing out how the value of 0.9 matches very well the value of η_0 derived in section 5.2 by means of an independent method.

The apparent albedo distribution of NEAs has been derived and compared to that of main belt asteroids. The mean albedo of the 46 objects listed in Table 4-6 is 0.27, which is much higher than the mean albedo of observed main-belt asteroids (~0.11). Further, results of this study are consistent with a trend of increasing albedo with decreasing size for S-type asteroids in the size range covered by our study (0.1 – 25 km). While we note that this apparent correlation may be real and reflect the lack of space weathering of small, young collision fragments, a selection effect in favor of the discovery and the follow-up of brighter asteroids cannot be ruled out. However, any detailed analysis of these selection effects is beyond the scope of this present work.

Finally, the statistics of albedos was calculated for the taxonomic classes represented in our sample of NEAs (see Table 5-2). Comparing the NEA albedo statistics with that derived by Bus (1999) for main belt asteroids, it appears that NEAs have higher albedos than MBAs. However, while S-type NEAs are on average 20% brighter than S-type MBAs, this difference is very striking for C-type objects: NEA C-types have on average albedos 57% higher than C-type MBAs.

Spectral type	p_V min	p_V max	p_V mean	StDev (p_V)	No. in sample	H mag for D=1km
S,Sq,Sr,Sl,Sk	0.14	0.52	0.27	0.08	20	17.0
S	0.14	0.52	0.28	0.09	17	17.0
C,B,F,Cb,Xc	0.05	0.16	0.11	0.04	7	18.0
Q	0.14	0.60	0.35	0.20	4	16.8
V	0.31	0.45	0.38	0.10	2	16.7
E	0.27	0.64	0.45	0.15	5	16.5
M	0.17	0.17	0.17	0.00	2	17.5
P	0.02	0.04	0.03	0.01	2	19.3

Table 5-2 Albedos statistics calculated for the taxonomic classes represented in our sample of NEAs

Our statistics allows an estimation of the albedo (and of the size, given the H value) to be obtained for those NEAs with known taxonomic type. Of course, this is not the case for E, M and P asteroids which are not distinguishable on the basis of spectroscopic observations.